Vis Comput
DOI 10.1007/s00371-017-1447-9

ORIGINAL ARTICLE

Role of normalization of breast thermogram images and automatic classification of breast cancer

Dayakshini Sathish[1] · **Surekha Kamath**[1] · **Keerthana Prasad**[2] · **Rajagopal Kadavigere**[3]

Abstract Breast thermography is a non-invasive imaging technique used for early detection of breast cancer based on temperatures. Temperature matrix of breast provides minute variations in temperatures, which is significant in early detection of breast cancer. The minimum, maximum temperatures and the their range may be different for each breast thermogram. Normalization of temperature matrices of breast thermograms is essential to bring the different range of temperatures to the common scale. In this article, we demonstrate the importance of temperature matrix normalization of breast thermograms. This paper also proposes a novel method for automatically classifying breast thermogram images using local energy features of wavelet sub-bands. A significant subset of features is selected by a random subset feature selection (RSFS) and genetic algorithm. Features selected by RSFS method are found to be relevant in detection of asymmetry between right and left breast. We have obtained an accuracy of 91%, sensitivity 87.23% and specificity 94.34% using SVM Gaussian classifier for normalized breast thermograms. Accuracy of classification between a set of hundred normalized and corresponding set of non-normalized breast thermograms are compared. An increase in accuracy of 16% is obtained for normalized breast thermograms in comparison with non-normalized breast thermograms.

Keywords Breast cancer · Breast thermography · Asymmetry analysis · Normalization · Wavelet local energy · Random subset feature selection · Genetic algorithm

✉ Surekha Kamath
surekha.kamath@manipal.edu

Dayakshini Sathish
dayakshini@gmail.com

Keerthana Prasad
keerthana.prasad@manipal.edu

Rajagopal Kadavigere
rajagopalkv@yahoo.com

[1] ICE Department, MIT Manipal, Manipal University, Manipal, Karnataka 576104, India

[2] SOIS Manipal, Manipal University, Manipal, Karnataka 576104, India

[3] KMC Manipal, Manipal University, Manipal, Karnataka 576104, India

1 Introduction

Breast cancer is the most commonly diagnosed cancer in women worldwide, accounting for 23% of total cancer cases and 14% of the cancer deaths [18]. The mortality rate of cancer can be reduced, if cancer is detected and treated at an early stage. Breast thermography can be used as an adjunct screening tool for early detection of breast cancer [26]. It is a painless, non-invasive, low cost screening test and can be used for women of all ages, particularly women having dense breast, where mammography is less effective [13,41].

Thermography is based on infra-red radiation of bodies with temperature higher than absolute zero. Infra-red radiation emitted by surface of body is captured by the thermal camera and is converted into corresponding temperature values. The thermal camera displays these temperature distributions as an image known as thermogram [21,39]. Cancerous tumors normally have higher metabolic activity and undergo angiogenesis, and hence, it has higher temperature in comparison to normal tissue [21,33]. These tumors in the breast rarely grow symmetrically in left and right breast, so physicians commonly use asymmetry analysis to interpret breast thermogram images [7,31,40]. Research on breast thermography shows that it can detect cancer at an early stage, when the physiological changes start in the breast, prior to

Published online: 20 October 2017

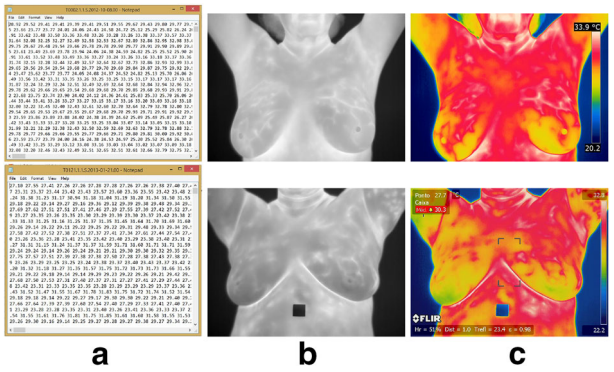

Fig. 1 Representation of breast thermograms **a** Temperature matrix **b** Grayscale image **c** Pseudo-color image

the growth of tumors. These physiological changes in the breast occur ten years earlier to the structural changes [10] and causes changes in the temperature distribution around the affected region [6,10].

Breast thermograms are usually represented in one of the three different forms namely temperature matrix, grayscale image and pseudo-color image (color mapped image). Screen shot of temperature matrix, grayscale image and pseudo-color image are shown for two patients in Fig. 1. Temperature matrix is a representation of temperature values of breast surface, sensed by the thermal camera. Grayscale image representation of thermogram image is formed by mapping the temperature values directly into pixel intensity range of 0–255. This type of direct mapping introduces error, since minimum and maximum temperatures and their range between minimum to maximum may be different for each thermogram [16]. Pseudo-color image is formed by mapping different colors for the range of temperature values. Color for each pixel depends on the color map and on the defined thresholds by the temperature scale for each image. Color mapping may vary from device to device [5,6]. Hence, it is important to use original temperature matrices rather than grayscale images (directly mapped) or pseudo-color images in order to accurately assess the changes occurring in the breast for asymmetry analysis.

As shown in Fig. 1 minimum, maximum and range between minimum to maximum differs for patient 1 and patient 2. Infra-red cameras generate thermal images by infra-red radiations and source of radiation is heat energy, temperature and heat exchange [16,21,39]. So thermogram images are highly sensitive with respect to variations in environmental, technical factors of camera, individual intrinsic and extrinsic factors [16]. Images used in the proposed work are collected from Database for Mastology Research (DMR) [30], which are captured in a highly controlled environment and are maintained for all the patients. Also high sensitive FLIR-SC620 thermal camera is used for all patients [36]. Even though the controlling parameters are strong in DMR, we observe the existence of large variations in temperatures(minimum and maximum) from patient to patient. These variations may be due to some of the uncontrollable parameters related to the body metabolic activity such as genetic factors, body weight, age and emotional factors etc. [16,38]. Also, there may be other environmental factors which are difficult to explore and may affect the breast temperature. Further, it is difficult to establish a testing environment with strict temperature control and consistency in each and every day of the year [38]. de Souza et al. [38] studied the effect of room and core body temperatures on breast thermograms. Their study showed that the breast temperature may vary with the room temperature, as well as with the metabolic activity of tissues and especially with the core body temperature. By considering all these factors, authors concluded that normalization of breast temperatures are essential to correct the room and body core temperature variations, which are influencing on breast temperatures. Normalization of breast temperature matrices makes the machine learning independent of all these factors. The next subsection discusses the research carried on development of computer-aided detection (CAD) for breast thermography along with the information on type of breast thermogram image used in their work.

1.1 Related work

Schaefera et al. [35] extracted various statistical and spectral features from manually segmented left and right breast thermogram images. The extracted features were fed to fuzzy classification system. Experimental results on a set of 150 cases attained an accuracy of classification of 80%, but details of the thermogram image were not specified in the paper. Araujo et al. [5] proposed interval symbolic feature extraction technique to account intrinsic variability of image data from the temperature matrix and obtained sensitivity of 85.7% and specificity of 86.5%. Borchartt et al. [8] computed mean, standard deviation, difference between maximum and minimum intensity features etc., from the region of interest (ROI) of pseudo-color thermogram image and obtained an accuracy of 86% using Support Vector Machine classifier. Acharya et al. [2] extracted texture features from co-occurrence matrix and run length matrix of pseudo-color thermogram image. Support vector machine (SVM) classifier was used for automatic classification of normal and malignant breast conditions. They obtained an accuracy of 88.1%, sensitivity and specificity of 85.71% and 90.48% respectively. In this work, the authors used 50 infrared breast images (25 normal and 25 cancer) collected from Singapore General Hospital Singapore. Acharya et al. [1] in another paper, extracted higher-order spectral features, namely entropy, phase (23°), entropy 1 (174°), entropy 2 (145°), mean of magnitude (114°), entropy 3 (56°), and entropy 2 (52°) by taking radon transform of pseudo-color

breast thermogram images. The authors used feed forward artificial neural network (ANN) and SVM classifiers for classifying the images as normal and abnormal thermograms. The higher-order spectral features with ANN presented better sensitivity, specificity and accuracy values of 92, 88 and 90%, respectively, in comparison with SVM. Nicandro et al. [27] extracted different types of features using temperature variations of breast, such as the temperature difference between left and right breast, number of veins with high temperature, heat area under the breast, number of hottest points, geometry of the hot center, histogram and age of the patient. Extracted features were classified using a Bayesian network classifier and they obtained an accuracy of 74%. However, they have not specified the type of thermogram image used in their work. Milosevic et al. [25] computed features based on Gray Level Co-occurrence Matrices (GLCM) from pseudo-color thermogram images. A total of twenty features were extracted from thermograms. Three types of classifiers namely SVM, Naive Bayes and K- nearest neighbor classifier were used. Classification performance was evaluated by fivefold cross validation and receiver operating characteristic analysis. K-nearest neighbor classifier performed better. Krawczyk et al. [19] analyzed breast thermograms based on image features and hybrid multiplier classifier system. They extracted various statistical features, temperature-based features and spectral features. The main objective of the authors was to develop a hybrid multiple classifier system for the effective classification of thermogram images. Images were segmented manually as left and right breast for asymmetry analysis. The design of a multiple classifier system was based on hybridization of three computationally intelligent techniques, namely neural network or SVM as base classifiers, neural fuser to combine the individual classifiers and Fuzzy measure for removing the redundant classifier from the ensemble. They obtained an average of 81.35% sensitivity, 90.66% specificity and an accuracy 88.79%. The details of thermogram images were not provided in their paper. Ali et al. [3] extracted first-order statistical and GLCM-based features from the automatically segmented ROI of grayscale breast thermogram images. SVM with various kernel functions were used to detect the normal and abnormal breasts. They analyzed accuracy of classifier results by using four types of scenarios. Each scenario had different number of images for training and testing. From their results, we find that first scenario (19 normal, 24 abnormal samples for training and 10 normal, 10 abnormal samples for testing) performed better than other scenarios. For statistical features quadratic and linear kernel gave an accuracy of 85% and for GLCM-based features quadratic and polynomial kernel gave an accuracy of 80%. Pramanik et al. [29] extracted statistical features from wavelet transform and used ANN for classification. Pseudo-color breast thermogram images were used in their work. Suganthi and Ramakrishnan [32] extracted Gabor wavelet transform-based features such as energy and amplitude. The results showed that normal and abnormal tissues resulted with maximum of 6% difference in average energy value at 150° orientation. Similarly, among the different pathological conditions, maximum variation is observed at 0° orientation. From the extracted features, anisotropy index and orientation measures were calculated to quantify the difference in texture energy. Twenty grayscale images present in the database [30] were used in their work.

2 Materials and methods

In the proposed research, breast temperature matrices are normalized prior to the image formation. Normalized breast thermograms are pre-processed and segmented automatically into right and left breast for asymmetry analysis [34]. Local energy features of wavelet sub-bands are extracted from the segmented breast thermograms. The absolute difference of features between right and left breast is obtained for the measurement of asymmetry. To reduce dimension of the feature space and to find the appropriate feature set, Sequential Floating Forward Feature Selection(SFFS), Random Subset Feature Selection (RSFS) and Genetic Algorithm (GA) are used. Selected features are fed to the classifier for training and testing. Local energy features of wavelet sub-bands selected by RSFS method attained a classification accuracy of 91% using SVM Gaussian classifier for normalized images and an accuracy of 75% is obtained from the corresponding set of non-normalized images. The block diagram representation of the above process is shown in Fig. 2.

2.1 Data collection

Breast thermogram images used in this proposed method are collected from the public database at Visual lab, Fluminense Federal University, Brazil [30]. One hundred frontal view static breast thermogram temperature matrices (47 abnormal, 53 normal) are considered for this study. Breast thermogram images are captured using FLIR infra-red camera with a temperature sensitivity of 0.04 °C and pixel resolution of 640 × 480 pixels. The population has a set of patients with confirmed tumor by clinical exam, ultrasound, mammography and biopsy exams [6,36].

2.2 Normalization of temperature matrices

In the proposed normalization method at first, we have recorded minimum and maximum temperatures of each breast temperature matrix present in the database [30]. Among all minimums and maximums, lowest minimum and highest maximum is recorded. Next, we have created a lookup table of temperature to intensity mapping such that

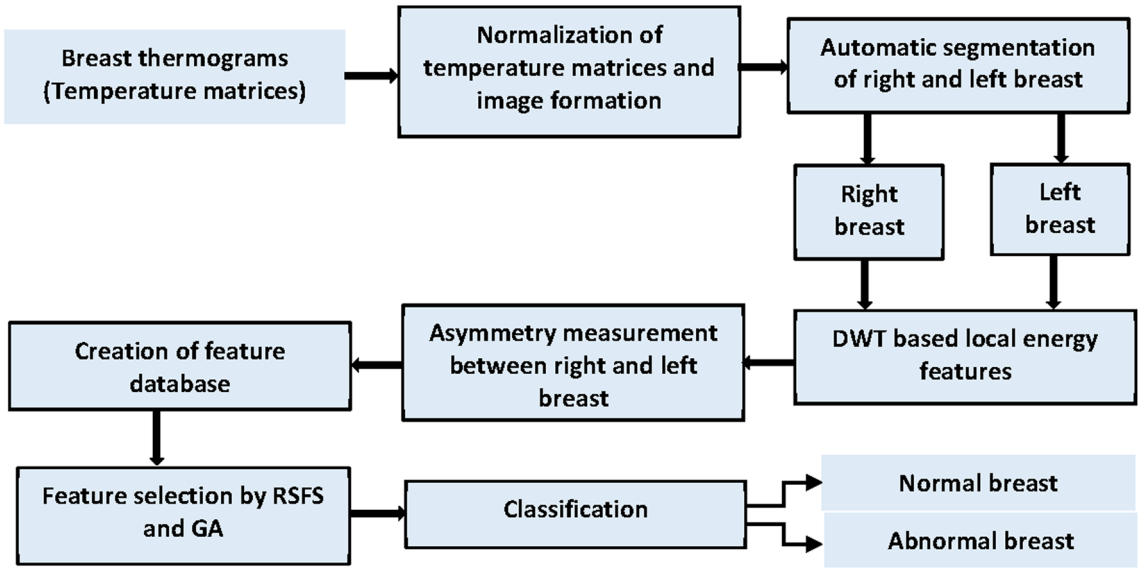

Fig. 2 Block diagram representation of the proposed work

lowest minimum temperature is mapped to 0 intensity value and highest maximum temperature is mapped to 255 intensity value. Since the temperature values have two decimal places, we have incremented the temperature values in the lookup table in steps of 0.01 °C. Now the normalized intensity value for each temperature increment is calculated by multiplying the incremental temperature step of 0.01 °C into the ratio of difference of maximum to minimum intensity to the difference of maximum to minimum temperature. The lookup table contains 1847 values of temperatures and their respective intensity values. Next, individual breast temperature matrix is converted into normalized grayscale image by mapping the values of the temperature matrix to respective normalized intensities by referring the lookup table. The proposed normalization algorithm is as follows:

Algorithm:

1. Find the minimum temperature of each breast temperature matrix of the individual say, $L1$, $L2$, $L3$. and so on.
2. Similarly, find the maximum temperature of each breast temperature matrix of the individual say, $H1$, $H2$, $H3$. and so on.
3. Among all minimums, find the lowest minimum say, L.
4. Among all maximums, find the highest maximum say, H.
5. Create a lookup table of temperature to intensity mapping, where lowest minimum L is mapped to zero intensity value and highest maximum H is mapped to intensity value of 255.
6. Intermediate temperature values with the increment of 0.01 °C are mapped to an intensity increment of I, where I is calculated as:

$$I = \frac{255}{(H - L)} * 0.01 \tag{1}$$

7. Consider each breast temperature matrix of the individual; from the lookup table search for intensity values of all temperature values and map the temperature values to its respective intensity values to obtain normalized grayscale image.
8. Save the normalized grayscale image in PNG format.
9. Repeat the steps 6 and 7 for all breast temperature matrices of database.

Temperature and pixel intensity values are computed from the temperature matrices and corresponding mapped images used in the proposed work are as follows:

1. Minimum temperature $M1 = 18.53$ °C and maximum temperature $M2 = 37.00$ °C has been found from all samples used in this work.
2. 1°C temperature is divided into 100 divisions in steps of 0.01 °C in the temperature matrix.
3. So, we obtain total temperature divisions of 1847 for temperature range of 18.53–37 °C.
4. Each temperature increment of 0.01 °C increases pixel intensity value by $I = 0.138$ in the lookup table.
5. For 1 °C temperature increment, increment the pixel intensity by $13.8 \approx 14$.

2.3 DWT-based features

The abnormal breast thermogram image textures may vary rapidly due to the presence of tumor, such variations in the texture are better captured by wavelet transforms. The nor-

malized breast thermograms are segmented automatically to separate right and left breast for asymmetry analysis, which is reported in [34]. The DWT of the segmented right and left image is obtained by filtering image through a series of digital filters at different scales. The scaling operation is done by changing the resolution of the image by a process of subsampling. The 2D DWT of an image $f(m,n)$ of size $M \times N$ is expressed as [15]:

$$W_\varphi(j_0,k,l) = \frac{1}{\sqrt{MN}} \sum_{m=0}^{M-1} \sum_{n=0}^{N-1} f(m,n)\varphi_{j_0,k,l}(m,n) \quad (2)$$

$$W_\psi^i(j,k,l) = \frac{1}{\sqrt{MN}} \sum_{m=0}^{M-1} \sum_{n=0}^{N-1} f(m,n)\psi_{j,k,l}^i(m,n) \quad (3)$$

where $i = \{H, V, D\}$ indicate the directional index of the wavelet function. j_0 represents any arbitrary starting scale, may be taken as zero. $W_\varphi(j_0,k,l)$ coefficients define an approximation of $f(m,n)$ at scale j_0. The $W_\psi^i(j,k,l)$ coefficients add horizontal, vertical and diagonal details for scales $j \geq j_0$. $\varphi_{j_0,k,l}(m,n)$ and $\psi_{j,k,l}^i(m,n)$ are scaling and wavelet functions, respectively, and defined as [15,17,37]:

$$\varphi_{j_0,k,l}(m,n) = 2^{\frac{j}{2}}\varphi(2^j m - k, 2^j n - l) \quad (4)$$

$$\psi_{j,k,l}^i(m,n) = \psi^i(2^j m - k, 2^j n - l), \quad i = \{H, V, D\} \quad (5)$$

It is possible to compute DWT through sub-band decomposition [15,24]. In case of sub-band analysis of image, we need extraction of its approximate forms in both horizontal and vertical directions. Further, detection of horizontal edges, detection of vertical edges and detection of diagonal edges are also essential. This 2-D analysis requires the use of following two-dimensional filter functions through the multiplication of separable scaling φ and corresponding wavelet functions ψ in m(horizontal) and n(vertical) directions, as defined below:

$$\varphi(m,n) = \varphi(m)\varphi(n) \quad (6)$$

$$\psi^H(m,n) = \psi(m)\varphi(n) \quad (7)$$

$$\psi^V(m,n) = \varphi(m)\psi(n) \quad (8)$$

$$\psi^D(m,n) = \psi(m)\psi(n) \quad (9)$$

With separable two-dimensional scaling and wavelet functions, we simply take one-dimensional DWT of the rows of $f(m,n)$, followed by the one-dimensional DWT of the resulting columns. Figure 3 shows the process in block diagram form. The 2D DWT filters the scale $j+1$ approximation coefficients to construct the scale j approximation and detail coefficients. Image $f(m,n)$ is used as the input to $W_\varphi(j,k,l)$. Convolving its rows with $h_\varphi(-l)$ and $h_\psi(-l)$ and down sampling its columns, we get two sub images whose horizontal resolutions are reduced by a factor of 2. The high-pass or detail component characterizes the image's high frequency information with vertical orientation; the low-pass, approximation component contains its low frequency vertical information. Both sub images are then filtered column-wise and downsampled to yield four quarter size output sub images W_φ, W_ψ^H, W_ψ^V, W_ψ^D.

In the proposed method, at first we have computed discrete wavelet transform of segmented right and left breast separately. All the sub-bands are considered for feature extraction, in order to incorporate coarse (LL sub-band) and fine variations in horizontal (LH), vertical (HL) and diagonal (HH) directions. Then we have computed the local energy (Norm-1) using 3×3 neighborhood, since it can capture all the local variations present in the image [4].The different texture patterns have different local energy distribution in the space frequency domain. Computation of local energy gives the finer texture details [4,42], which are essential for early detection of breast cancer. Also the lesions or changes in vascular pattern in the breast thermogram image are highlighted by wavelet local energies. Six basis functions are used for the analysis of breast thermogram images. They are Daubechies-1, Daubechies-10, Coiflet-1, Coiflet-5, Symlet-

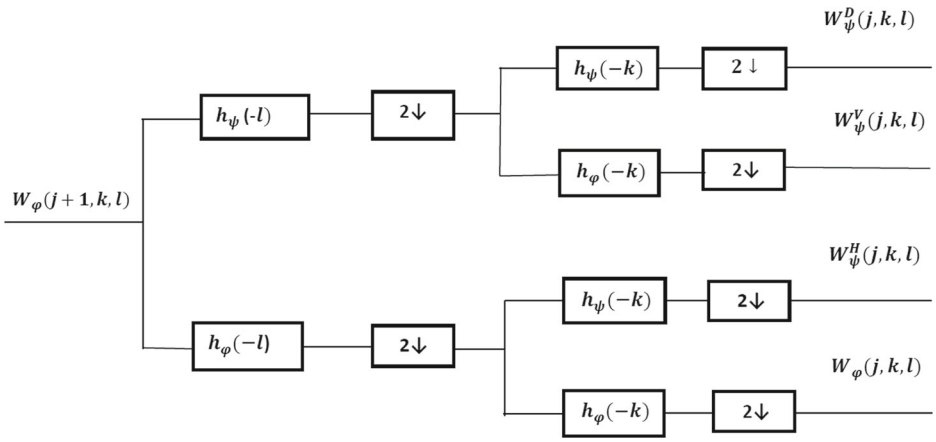

Fig. 3 2-D Analysis filtering through separable scaling and wavelet functions

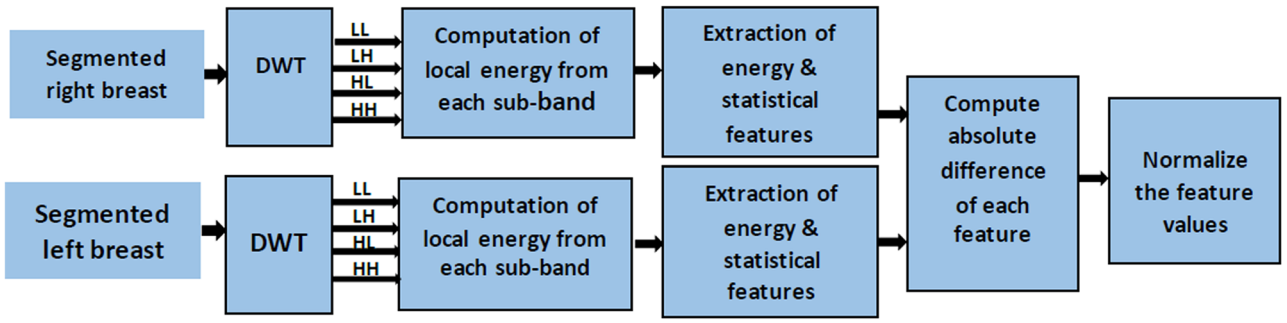

Fig. 4 Feature extraction using local energies of wavelet sub-bands

2 and Symlet-8. Wavelets are selected based on experiments by considering maximum intra variability in the feature values. Wavelet functions with one low and one high vanishing moments are used, so that all the smoother and sparse textures are captured for the analysis. Local energy calculation of ith sub-band is as follows:

$$L_i(k,l) = \frac{1}{9}\sum_{u=0}^{2}\sum_{v=0}^{2}|W_i(k-1+u, l-1+v)|^2 \tag{10}$$

where $W(k,l)$ is the wavelet transformation coefficient at location (k,l) in the ith sub-band. The wavelet transformation coefficient at the center of each 3×3 neighborhood is replaced with corresponding local energy. From the local energy of the wavelet sub-bands, we have computed energy and five statistical features namely mean, variance, skewness, kurtosis and entropy. The block diagram representation of feature extraction technique is shown in Fig. 4.

The mathematical equations for the computations of energy and five statistical features from the local energies of ith sub-band are given below.

$$\text{Energy}(E) = \sum_{k=1}^{p}\sum_{l=1}^{q} L_i(k,l) \tag{11}$$

where p, q are the number of rows and columns of the i^{th} sub-band respectively.

$$\text{Mean}\ (\mu) = \frac{1}{pq}\sum_{k=1}^{p}\sum_{l=1}^{q} L_i(k,l) \tag{12}$$

$$\text{Variance}\ (\sigma^2) = \frac{1}{(p-1)(q-1)}\sum_{k=1}^{p}\sum_{l=1}^{q}(L_i(k,l)-\mu)^2 \tag{13}$$

$$\text{Skewness}\ (S) = \frac{1}{pq}\sum_{k=1}^{p}\sum_{l=1}^{q}\frac{(L_i(k,l)-\mu)^3}{\sigma^3} \tag{14}$$

$$\text{Kurtosis}\ (K) = \frac{1}{pq}\sum_{k=1}^{p}\sum_{l=1}^{q}\frac{(L_i(k,l)-\mu)^4}{\sigma^4} \tag{15}$$

Table 1 Asymmetry measure of features extracted from local energies of ith sub-band

Feature	Features extracted from right breast	Features extracted from left breast	Asymmetry measure
Energy (E)	E_R	E_L	$E = \lvert E_R - E_L \rvert$
Mean (μ)	μ_R	μ_L	$\mu = \lvert \mu_R - \mu_L \rvert$
Variance (σ^2)	σ_R^2	σ_L^2	$\sigma^2 = \lvert \sigma_R^2 - \sigma_L^2 \rvert$
Skewness (S)	S_R	S_L	$S = \lvert S_R - S_L \rvert$
Kurtosis (K)	K_R	K_L	$K = \lvert K_R - K_L \rvert$
Entropy (ET)	ET_R	ET_L	$\text{ET} = \lvert \text{ET}_R - \text{ET}_L \rvert$

$$\text{Entropy (ET)} = -\sum_{k=1}^{p}\sum_{l=1}^{q} L_i(k,l)Log(L_i(k,l)) \tag{16}$$

All these features are extracted separately from wavelet transformed local energies of right and left breast. Next, we measure the asymmetry between right and left breast by computing the absolute difference of each feature between right and left breast from the respective sub-bands. The details of asymmetry measure of each feature between right and left breast for any sub-band is shown in Table 1.

After measuring the asymmetry, feature values are normalized by finding maximum value of asymmetry measure of all samples for each feature and then divide each sample by its maximum value obtained for corresponding feature.

2.4 Feature selection and classification

To obtain high performance from the classifiers, it is essential to provide an appropriate and compact feature set to the classifiers [12,20]. The performance of the classifier is tested by choosing three types of feature selectors namely SFFS, RSFS and GA. In SFFS method, feature subset is first enhanced by l features using forward selection and then r features are deleted using backward selection. The number of forward and backward steps is determined dynamically while the method

is running so as to maximize the criterion function. At each step, only a single feature is added or removed. The values of l and r kept floating, i.e., they are kept flexible so as to approximate the optimal solution as much as possible. Consequently, the dimensionality of the feature subset does not change monotonically but is actually floating up and down. RSFS method discovers a set of good features obtained by recursively selecting a random subset of features from the set of all possible features and then classifying the data. During each iteration, the relevance of each feature is adjusted according to the classification performance of the subset that the feature participates in. As more iterations are performed, the quality of the feature set gradually improves since random components in the selection process become averaged out [28]. RSFS method selects thirty six best features using forty iterations. GA works with a set of candidate solutions called a population and obtains optimal solution after a series of iterative computations. GA evaluates each individual's fitness through a fitness function [23,43]. Eighty generations are used for selecting twelve significant features.

Support vector machines are developed from statistical learning theory. SVMs maximize the margin around the separating hyperplane. The decision function is fully specified by a subset of training samples and support vectors [1,12]. To reduce the curse of dimensionality, SVM with four kernel functions are tested namely linear, Gaussian, polynomial and quadratic [9,12,37]. $k$fold cross validation with k=5 is used to evaluate the performance of the classifiers. Average value of accuracy, sensitivity and specificity are computed by running the $k$fold validation hundred times.

3 Results and discussions

In this section, we demonstrate and discuss normalization results and automatic classification of normalized and non-normalized breast thermogram images.

3.1 Normalization of temperature matrices

In order to find the significance of temperature matrix normalization, we consider 1 °C temperature difference in breast thermograms. It is observed that, intensity level considerably changes for a temperature difference of 1 °C in non-normalized grayscale images, whereas it remains constant in normalized gray scale images. This is due to the fact that, in non- normalized gray scale images, temperatures are directly mapped to gray intensity levels.

Table 2 presents the amount of intensity difference for 1 °C temperature difference within the breast image for non-normalized and normalized grayscale images. In Table 2, we consider two pixels with temperature difference of 1 °C,

Table 2 Amount of intensity difference (D) for a temperature difference ($T1 - T2$) of 1 °C in non- normalized and normalized gray images

Image ID	x_1, y_1	$T1$	x_2, y_2	$T2$	Non-normalized grayscale images			Normalized grayscale images		
					I1	I2	D	I1	I2	D
ID 1	569, 56	31	150, 198	30	186	169	17	172	158	14
	469, 494	31	472, 146	30	187	171	16	172	158	14
	12, 99	24.46	13, 574	25.46	75	94	19	82	96	14
	457, 117	24.46	456, 119	25.46	77	94	17	82	96	14
	469, 611	21.28	466, 119	22.28	20	40	20	38	52	14
	478, 123	21.28	472, 128	22.28	22	39	17	38	52	14
	284, 103	25.00	430, 552	26.00	88	102	14	89	103	14
	467, 519	25.00	318, 93	26.00	87	100	13	89	103	14
	477, 372	33.45	435, 363	34.45	231	246	15	206	220	14
	445, 330	33.45	459, 403	34.45	228	246	18	206	220	14
ID 269	454, 538	25.00	13, 392	26.00	32	47	15	89	103	14
	425, 540	25.00	369, 92	26.00	32	49	17	89	103	14
	474, 50	23.78	480, 541	24.78	8	29	21	72	86	14
	408, 7	23.78	426, 560	24.78	8	28	20	72	86	14
	474, 95	30.10	44, 401	29.10	134	108	26	160	146	14
	1, 251	30.10	203, 81	29.10	126	115	11	160	146	14
	98, 523	35.35	292, 121	34.35	236	216	20	232	218	14
	114, 63	35.35	455, 177	34.35	232	214	18	232	218	14
	470, 110	32.88	465, 175	33.88	186	205	19	198	212	14
	477, 116	32.88	456, 147	33.88	185	205	20	198	212	14

have coordinates $x1$, $y1$ and $x2$, $y2$. $I1$ and $I2$ denote the intensity values for temperatures $T1$ (at $x1$, $y1$) and $T2$ (at $x2$, $y2$), respectively. $D\,(I1 - I2)$ indicates the intensity difference obtained for 1 °C difference in temperature. Also ID1 and ID 269 represent normal and abnormal breast thermogram image respectively. As presented in Table 2, for non-normalized grayscale images, 1 °C temperature difference results in distinct D values for image ID1 and ID269 due to variation in minimum, maximum temperature and their range. The value of D remains constant within the normalized grayscale image and also for all normalized samples.

Table 3 provides normalization results obtained for 20 breast thermograms (10 normal and 10 abnormal cases). The minimum, maximum temperatures and intensity values of each image are shown in Table 3. Intensity values are noted for two pixels with a temperature difference of 1 °C. Range of intensity difference for 1 °C temperature difference is provided for non-normalized grayscale images. From Table 3, we observe that range of intensity difference varies from image to image in non-normalized grayscale images, whereas it remains constant (14 in Table 2) for all normalized gray scale images.

It is observed from the related work that many research groups have used pseudo-color images [1,2,14,25,27,29], grayscale images [3,32] and also some groups have not provided any information on the type of breast thermogram used [19,27,35]. The accuracy of classification of breast thermogram images depends on various factors, namely the type of breast thermogram used (pseudo-color image, grayscale image or original temperature matrix), number of samples, segmentation, extracted features and classifier used. Each and every factor is essential in the analysis of breast thermograms. Araujo et al. [5] described the importance of original temperature matrices rather than pseudo-color images.

Normalization of temperature matrices is essential to bring the temperature range of each patient to common scale. Few articles namely Brioschi et al. [11], Lashkari et al. [22] and de Souza et al. [38] reported the significance of normalization of breast thermograms. The objective of proposed normalization method is to develop machine learning independent of various factors influencing on the temperature variations in the breast. Also, we need to develop computer-aided detection for breast thermography for images captured at different locations that can be validated for investigating diseases by comparison, without the need for adaptation to maintain the

Table 3 Range of intensity change for a temperature difference of 1 °C for a set of 20 non-normalized and normalized grayscale images

Image ID	Minimum temperature	Maximum temperature	Non-normalized grayscale image			Normalized grayscale image		
			Minimum intensity	Maximum intensity	Range of intensity change	Minimum intensity	Maximum intensity	Intensity change
1	20.00	34.95	2	255	14–21	20	227	14
6	19.86	35.37	1	252	13–20	18	232	14
13	21.17	35.72	1	255	15–21	36	237	14
15	20.71	35.65	1	254	13–20	30	250	14
19	20.56	34.32	2	254	15–21	28	218	14
20	20.41	35.86	2	255	13–20	26	239	14
26	19.94	35.27	0	255	12–19	19	231	14
28	20.06	34.58	3	255	15–20	21	222	14
75	21.30	34.02	3	254	17–25	38	214	14
98	20.19	35.08	0	255	13–20	23	228	14
198	21.82	35.73	1	255	16–22	45	237	14
242	20.57	35.35	0	255	14–19	28	232	14
246	19.93	36.89	2	255	12–16	19	253	14
255	22.36	35.02	1	255	17–26	44	219	14
259	23.04	36.94	1	254	16–21	62	254	14
260	23.05	36.34	2	255	17–21	62	246	14
266	22.52	36.52	3	255	16–21	55	248	14
267	22.72	35.81	1	255	17–22	58	239	14
268	22.46	35.12	1	255	17–25	54	229	14
269	23.34	36.35	0	255	17–25	66	246	14

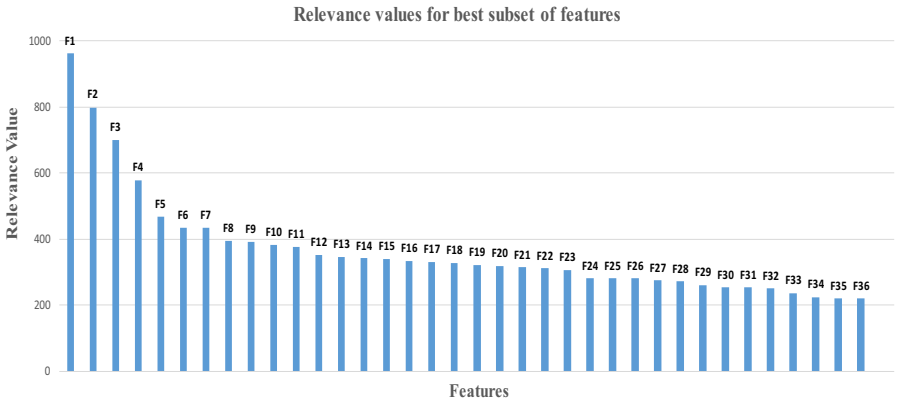

Fig. 5 Relevance values for best subset of features selected by RSFS method for normalized breast thermograms

Table 4 Features selected by RSFS method for normalized breast thermograms

Wavelet	Sub-bands	Selected Features
DB 10	LH	Entropy(F20)
	HL	Entropy(F9)
	LL	Mean(F29), Energy(F31)
DB 1	HL	Entropy(F1)
	LL	Mean(F11), Kurtosis(F14), Entropy(F17), Variance(F26)
Coiflet 5	HL	Entropy(F15)
	HH	Entropy(F2), Energy(F23)
	LL	Mean(F16), Kurtosis(F19), Energy(F33)
Coiflet 1	LH	Entropy(F28)
	HL	Entropy(F32)
	HH	Energy(F8)
	LL	Mean(F12), Energy(F25), Kurtosis(F30)
Symlet 8	LH	Entropy(F3)
	HH	Entropy(F22), Energy(F24)
	LL	Mean(F10), Variance(F21), Energy(F27)
Symlet 2	LH	Entropy(F18)
	HL	Entropy(F6)
	HH	Entropy(F4), Energy(F13)
	LL	Kurtosis(F5), Mean(F7)

same consistent temperature during the whole year. It is necessary to mathematically correct the temperature variations to compare with the published studies. It is essential to obtain reliable and independent analysis of the patients with respect to environmental and metabolic conditions in different data acquisition scenarios. Future research on this can be investigated on the above factors.

3.2 Automatic classification of breast thermograms

Wavelet sub-band energy features can amplify the amplitude variation between regions. Global energy uses the visual features of the whole image, while local energy takes into account the regions or objects to describe the image. The subset of local energy features of wavelet sub-bands, selected by RSFS method performed better in comparison with GA and SFFS methods. For normalized breast thermograms, RSFS method selects a combination of thirty six features from the set of one hundred and forty four features extracted from the local energies of wavelet sub-bands. Twelve entropy and four energy features extracted from the local energies of wavelet high-pass sub-bands are highly relevant for classification of normal breast versus abnormal breast. RSFS also selects seventeen statistical features from the low-pass sub-bands. Figure 5 shows the bar chart of relevance values of best subset of features selected by RSFS method for normalized breast thermograms. The selected features are sorted in descending order based on the relevance value as shown in Fig. 5. Feature F1 (Entropy of HL sub brand of DB1) gets the highest relevance value. The features selected by RSFS method are shown in Table 4 for normalized breast thermo-

Table 5 Comparison of normalized and non-normalized breast thermograms using different combination of classifiers and feature selectors

Classifier	Feature selector	Performance					
		Normalized			Non-normalized		
		Accuracy (%)	Sensitivity (%)	Specificity (%)	Accuracy (%)	Sensitivity (%)	Specificity (%)
SVM linear	None	76	61.7	88.6	65	53.19	75.5
	SFFS	69	53.2	83	66	55.3	75.4
	RSFS	89	83	94.3	72	61.7	81.1
	GA	86	76.6	94.3	64	55.31	71.69
SVM Gaussian	None	78	72.3	83	65	48.93	79.2
	SFFS	78	89.36	67.9	75	79.2	70.2
	RSFS	91	87.23	94.34	75	65.9	83.0
	GA	84	78.72	88.67	67	57.4	75.47
SVM Polynomial	None	75	70.2	79.2	61	48.9	71.7
	SFFS	76	74.5	77.3	74	61.7	84.9
	RSFS	85	74.5	94.3	70	55.3	83.0
	GA	75	66	83	50	42.5	56.6
SVM Quadratic	None	74	65.9	81.1	59	48.9	67.9
	SFFS	77	72.3	81	75	66	83
	RSFS	86	76.6	94.3	75	63.8	84.9
	GA	80	74.5	85	56	42.5	67.9

Table 6 Comparison of classifier performance between normalized and non-normalized images using texture features [2] and wavelet features (proposed method)

Breast thermograms	Classifier performance					
	Texture features			Wavelet features (Proposed method)		
	Accuracy (%)	Sensitivity (%)	Specificity (%)	Accuracy (%)	Sensitivity (%)	Specificity (%)
Normalized	72	79.24	63.82	91	87.23	94.34
Non-normalized	65	68	62.3	75	65.9	83.0

grams. Thirty six features are selected by RSFS method for non-normalized images.

Classification results of SVM classifier with linear, Gaussian, polynomial and quadratic kernels are tested with different combination of features selected by SFFS, RSFS and GA using k fold cross validation with k =5. Comparison of performance of the classifiers for normalized and corresponding set of non-normalized thermograms with different combination of feature selectors are shown in Table 5. It is observed from Table 5 that, SVM Gaussian kernel performed better in comparison with other kernel functions. High accuracy of 91% is obtained by SVM Gaussian with RSFS method for normalized breast thermograms. Non-normalized breast thermograms provide only 75% of maximum accuracy for the best set of features selected by RSFS method using SVM Gaussian classifier. There is a 16% increase in the classification accuracy, 21.33% sensitivity and 11.34% specificity for normalized breast thermograms in comparison with the corresponding set of non-normalized breast thermograms. The results obtained by the proposed method signifies the need for temperature matrix normalization prior to the image formation to analyze the breast thermograms for early detection.

We have also compared the proposed method with the method proposed by Acharya et al. [2] using texture features extracted from co-occurrence matrix and run length matrix for normalized and non-normalized thermograms. Images are segmented as right and left breast using [34]. Statistical t test is used for selecting the significant features. SVM Gaussian classifier is used for classification. Classifier performance is evaluated using $k$fold cross validation. Table 6 depicts the comparison of classifier performance between normalized and non-normalized breast thermograms for texture features [34]. As shown in Table 6, proposed method performs better in comparison with the texture features method [34]. Also, in both the methods, normalized breast thermograms performed better in comparison with the non-normalized thermograms indicating the importance of normalization.

Table 7 Similar studies on detection of breast cancer using breast thermogram images

Authors	No. of samples	Type of Breast thermogram image	Segmentation method	Extracted features	Feature selection	Classifier	Performance
Araujo et al. [5]	50 (14 malignant19 benign 17 cyst)	Temperature matrices and grayscale image	Semi-automated	Interval symbolic feature extraction on temperature values	–	Distance based classifier	Sensitivity:85.7% Specificity:86.5%
Ali et al. [3]	63 (29 normal, 34 abnormal)	Grayscale images from database	Automatic	Statistic GLCM features	*t* test	SVM with Kernels	Accuracy: Statistic :85% GLCM:80%
Acharya et al. [2]	50 (25 normal, 25 cancer)	Pseudo-color images	Manual cropping	Texture features(RLM and Co-occurence)	–	SVM	Accuracy:88.10%
Acharya et al. [1]	50 (25 normal, 25 cancer)	Pseudo-color images	Manual cropping	Higher-order spectral features	*t* test	ANN SVM	Accuracy ANN: 90% SVM: 80%
Schaefera et al. [13]	146 (29 malignant,117 benign)	Not specified	Manual	Statistical / spectral features	GA	Fuzzy rule based	Accuracy: 80%
Borchartt et al. [27]	28 (24 abnormal,4 normal)	Pseudo-color images	Automatic	Statistical temperature features	–	SVM	Accuracy: 85.7%
Nicandro et al. [6]	98 (77 malignant, 21 healthy)	Not specified	Not specified	Temperature features	–	Naive Bayes classifier	Accuracy: 71.88%
Milosevic et al. [25]	40 (26 normal, 14 abnormal)	Pseudo-color images	Semi-automated	GLCM	–	SVM Naive Bayes KNN	Accuracy SVM: 85% Naive Bayes : 80% KNN: 92.5%
Krawczyk et al. [19]	146 (29 malignant, 117 benign)	Not specified	Manual	Statistical / spectral features	Fast correlation-based feature filter	Hybrid multiple (NN with SVM)	Accuracy: 88.79%
Proposed method	100 (47 abnormal, 53 normal)	Normalized grayscale images	Automatic	Wavelet local energy features	RSFS	SVM Gaussian	Accuracy: 91% Sensitivity: 87.23% Specificity: 94.34%

The proposed method extracts features from the local energy distributions of wavelets. These conventional wavelets transforms are simpler and take lesser computation time as compared with other feature extraction techniques. Also local energy features are able to distinguish the asymmetry between right and left breast in abnormal breast thermograms. We have obtained an accuracy of 91% for set of hundred images using local energy features. Feature selection by RSFS method also plays an important role by selecting the best subset of features as per the relevant values of features computed using classification performance. A summary of similar works carried on detection of breast cancer is presented in Table 7.

4 Conclusion

This article proposes a novel method for early detection of breast cancer in women. We have demonstrated the need for normalization of breast temperature matrices prior to the image formation. The Wavelet-based local energy features are found to be highly significant in differentiating normal and abnormal breast. The proposed method compares the accuracy of classification between normalized and non-normalized images using two types of feature selection methods, namely RSFS and GA. RSFS method selected a best combination of feature subset and we have obtained 91% of accuracy of classification, using SVM Gaussian classifier for normalized breast thermogram images. Increase in accuracy of 16% is found in normalized breast thermogram images in comparison with the non-normalized breast thermograms. Future work could be verifying accuracy of classification for different degrees of malignancy with large number of datasets.

References

1. Acharya, U.R., Ng, E.Y.K., Sree, S.V., Chua, C.K., Chattopadhyay, S.: Higher order spectra analysis of breast thermograms for the automated identification of breast cancer. Expert Syst. **31**(1), 37–47 (2014)
2. Acharya, U.R., Ng, E.Y.K., Tan, J.H., Sree, S.V.: Thermography based breast cancer detection using texture features and support vector machine. J. Med. Syst. **36**(3), 1503–1510 (2012)
3. Ali, M.A.S., Sayed, G.I., Gaber, T., Hassanien, A.E., Snasel, V., Silva, L.F.: Detection of breast abnormalities of thermograms based on a new segmentation method. In: Proceedings of the Federated Conference on Computer Science and Information Systems(FedCSIS), vol. 5, pp. 255–261. IEEE (2015). doi:10.15439/2015F318
4. Amirolad, A., Arashloo, S.R., Amirani, M.C.: Multi-layer local energy patterns for texture representation and classification. Vis. Comput. **32**(12), 1633–1644 (2016)
5. Araujo, M.C.D., de Lima, R.C.F., de Souza, R.M.C.R.: Interval symbolic feature extraction for thermography breast cancer detection. Expert Syst. Appl. **41**(15), 6728–6737 (2014)
6. Araujo, M.C.D., Lima, R.D.C.F.D., Magnani, F.S., da Silva, R.N.T., dos Santos, F.G.: The use of a database as an auxiliar tool in thermographic diagnosis for early detection of breast diseases. In: 12th Brazilian Congress of Thermal Engineering and Sciences, Belo Horizonte, MG (2008)
7. Borchartt, T.B., Conci, A., de Lima, R.C.F., Resmini, R., Sanchez, A.: Breast thermography from an image processing view point: a survey. Int. J. Signal Process. **93**(10), 2785–2803 (2013)
8. Borchartt, T.B., Resmini, R., Conci, A.: Thermal feature analysis to aid on breast disease diagnosis. In: 21st Brazilian Congress of Mechanical Engineering, Natal, RN, Brazil, Proceedings of COBEM, ABCM, pp. 24–28 (2011)
9. Berbar, M.A.: Three robust features extraction approaches for facial gender classification. Vis. Comput. **30**(1), 19–31 (2014)
10. Bezerra, L.A., de Oliveira, M.M., Rolim, T.L., Conci, A., Santos, F.G.S., Lyra, P.R.M., de Lima, R.C.F.: Estimation of breast tumor thermal properties using infrared images. Signal Process. **93**(10), 2851–2863 (2013)
11. Brioschi, M.L., Matias, J.E.F., Teixeira, M.J., Vargas, J.V.: Automated computer diagnosis of IR medical imaging. FLIR Tech. Ser. Appl. Note Res. Sci. **8**(11), 1–6 (2011)
12. Devi, V.S., Murty, M.N.: Pattern Recognition Introduction, 2nd edn. Universities Press (India) Private Limited, Hyderabad (2013)
13. EtehadTavakol, M., Chandran, V., Ng, E.Y.K., Kafieh, R.: Breast cancer detection from thermal images using bispectral invariant features. Int. J. Therm. Sci. **69**(1), 21–36 (2013)
14. Gogoi, U.R., Majumdar, G., Bhowmik, M.K., Ghosh, A.K., Bhattacharjee, D.: Breast abnormality detection through statistical feature analysis using infrared thermograms. In: International Symposium on Advanced Computing and Communication (ISACC) Silchar, India, pp. 258–265. IEEE (2015)
15. Gonzalez, R.C., Woods, E.R.: Digital Image Processing, 2nd edn. Pearson Education (Singapore) Pte. Ltd., Delhi (2005)
16. Ismael, F.C., Carlos, B.M.J., Javier, A.L., Maria, G.C.P., Sergio, P.C., Angel, G.C.M., Manuel, S.Q.: Classification of factors influencing the use of infrared thermography in humans a review. Infrared Phys. Technol. **71**, 28–55 (2015)
17. Jayaraman, S., Esakkirajan, S., Veerakumar, T.: Digital Image Processing, 1st edn. Tata McGraw Hill Education Private Limited, New Delhi (2012)
18. Jemal, A., Bray, F., Center, M.M., Ferlay, J., Ward, E., Forman, D.: Global cancer statistics. Cancer J. Clin. **61**(2), 69–90 (2011)
19. Krawczyk, B., Schaefer, G.: A hybrid classifier committee for analysing asymmetry features in breast thermograms. Appl. Soft Comput. **20**(Special issue), 112–118 (2014)
20. Kumar, V., Minz, S.: Feature selection: a literature review. Smart Comput. Rev. **4**(3), 211–229 (2014)
21. Lahiri, B.B., Subramainam, B., Jayakumar, T., Philip, J.: Medical applications of infrared thermography: a review. Infrared Phys. Technol. **55**(4), 221–235 (2012)
22. Lashkari, A., Pak, F., Firouzmand, M.: Full intelligent cancer classification of thermal breast images to assist physician in clinical diagnostic applications. J. Med. Signals Sens. **6**(1), 12–24 (2016)
23. Ludwig, O., Nunes, U.: Novel maximum margin training algorithms for supervised neural networks. IEEE Trans. Neural Netw. **21**(6), 972–984 (2010)
24. Martis, R.J., Chakraborty, C., Ray, A.K.: Wavelet-based machine learning techniques for ECG signal analysis. In: Dua S (ed) Machine Learning in Healthcare Informatics, Intelligent Systems Reference Library, vol. 56, pp. 25–45. Springer (2014)
25. Milosevic, M., Jankovic, D., Peulic, A.: Thermography based breast cancer detection using texture features and minimum variance quantization. EXCLI J. **13**, 1204–1215 (2014)

26. Ng, E.Y.K., Sudharsan, N.: Computer simulation in conjunction with medical thermography as an adjunct tool for early detection of breast cancer. BMC Cancer **4**, 17 (2004)
27. Nicandro, C.R., Efren, M.M., Yaneli, A.A., Enrique, M.D.C.M., Gabriel, A.M.H., Nancy, P.C., Alejandr, G.H., de Jesus, H.R.G., Rocio, B.M.: Evaluation of the diagnostic power of thermography in breast cancer using bayesian network classifiers. Comput. Math. Methods Med. **2013**(5), 1–10 (2013)
28. Pohjalainena, J., Rsnena, O., Kadioglu, S.: Feature selection methods and their combinations in high dimensional classification of speaker likability, intelligibility and personality traits. Comput. Speech Lang. **29**(1), 145–171 (2015)
29. Pramanik, S., Bhattacharjee, D., Nasipuri, M.: Wavelet based thermogram analysis for breast cancer detection. In: International Symposium on Advanced Computing and Communication (ISACC) Silchar, India, pp. 205–212. IEEE (2015)
30. PROENG: Image processing and image analysis applied to mastology. http://visual.ic.uff.br/en/proeng (2015). Accessed 5 Oct 2015
31. Qi, H., Snyder, W.E., Head, J.F., Elliott, R.L.: Detecting breast cancer from infrared images by asymmetry analysis. In: Engineering in Medicine and Biology Society Proceedings of the 22nd Annual International Conference of the IEEE , Chicago, IL, vol. 2, pp. 1227–1228 (2000)
32. Suganthi, S.S., Swaminathan, R.: Analysis of breast thermograms using gabor wavelet anisotropy index. J. Med. Syst. **38**(9), 101 (2014). doi:10.1007/s10916-014-0101-6
33. Sathish, D., Kamath, S., Kadavigere, R., Prasad, K.: Medical imaging techniques and computer aided diagnostic approaches for the detection of breast cancer with an emphasis on thermography a review. Int. J. Med. Eng. Inform. **8**(3), 275–299 (2016)
34. Sathish, D., Kamath, S., Prasad, K., Kadavigere, R.: Asymmetry analysis of breast thermograms using automated segmentation and texture features. Signal Image Video Process. **11**(4), 745–752 (2017). doi:10.1007/s11760-016-1018-y
35. Schaefera, G., Zavisek, M., Nakashima, T.: Thermography based breast cancer analysis using statistical features and fuzzy classification. Pattern Recognit. **47**(6), 1133–1137 (2009)
36. Silva, L.F., Saade, D.C.M., Olivera, G.O.S., Silva, A.C., Paiva, A.C., Bravo, R.D., Conci, A.: A new database for breast research with infrared image. J. Med. Imaging Health Inform. **4**(1), 92–100 (2014)
37. Sonka, M., Hlavac, V., Boyle, R.: Image Processing, Analysis and Machine Vision, 2nd edn. Thomson Learning, Brooks/Cole Publishing Company, Pacific Grove, California (2004)
38. de Souza, G.A.G.R., Brioschi, M.L., Vargas, J.V.C., Morais, K.C.C., Neto, C.D., Neves, E.B.: Reference breast temperature: proposal of an equation. Einstein (Sao Paulo) **13**(4), 518–524 (2015)
39. Subramainam, B., Lahiri, B.B., Saravanan, T., Philip, J., Jayakumar, T.: Infrared thermography for condition monitoring a review. Infrared Phys. Technol. **60**, 35–55 (2013)
40. Tang, X., Ding, H.: Asymmetry analysis of breast thermograms with morphological image segmentation. In: Proceedings of the 2005 IEEE Engineering in Medicine and Biology 27th Annual Conference Shanghai, China, pp. 1680–1683. IEEE (2005)
41. Thermology, of Clinical, A.C.: Breast thermography. http://www.thermologyonline.org (2015). Accessed 19 Jan 2015
42. Tuytelaars, T., Mikolajczyk, K.: Local invariant feature detectors: a survey. Found. Trends Comput. Graph. Vis. **3**(3), 177–280 (2007)
43. Zhuo, L., Zheng, J., Wang, F., Li, X., Ai, B., Qian, J.: A genetic algorithm based wrapper feature selection method for classification of hyperspectral images using support vector machine. Int. Arch. Photogramm. Remote Sens. Spat. Inf. Sci. **XXXVII**, 397–402 (2015)

Dayakshini Sathish obtained her B.E. in Electronics and Communication Engineering from Mangalore University and her M.Tech. degree in Digital Electronics and Communication Engineering from Visvesvaraya Technological University Belgaum. Currently pursuing her Doctoral degree at Manipal Institute of Technology, Manipal University, Manipal. She has got nearly 15 years of teaching experience and 3 years of research experience in the field of Electronics and Communication Engineering. Her areas of interest include Digital Image Processing, Signal processing and Digital communications. Presented and published 20 research papers in conferences and reputed journals.

Surekha Kamath is currently working as an Associate Professor in the department of Instrumentation and Control Engineering at Manipal Institute of Technology, Manipal University, Manipal. She has got more than 23 years of teaching experience. She has published more than 60 research papers in various International/National Journals and conferences. Her areas of interests are Biomedical Signal and Image Processing and Bio Control Systems.

Keerthana Prasad is presently working as an Associate Professor in the department of School of Information Sciences Manipal University, Manipal. She has got more than 20 years of teaching and research experience. She has published many research papers in various International/National Journals and conferences. Her areas of interest are Medical Image Processing and Signal Processing.

Rajagopal Kadavigere is currently working as a Professor and Head of the Department of Radio diagnosis, Kasturba Medical College and Hospital, Manipal University, Karnataka, India. He has got more than 23 years of experience in the field of teaching/research. He has published research papers in various International/National Journals and conferences. His areas of interest are Musculoskeletal Imaging, GI Radiology, Neuroradiology, Breast Imaging etc.